Sensitivity of tropical cyclone models to the surface drag coefficient in different boundary-layer schemes

Roger K. Smith[a], Michael T. Montgomery[b], and Gerald L. Thomsen[a]

[a] *Meteorological Institute, University of Munich, Munich, Germany* [b] *Dept. of Meteorology, Naval Postgraduate School, Monterey, CA & NOAA's Hurricane Research Division*

*Correspondence to: Roger K. Smith, Meteorological Institute, University of Munich, Theresienstrasse 37, 80333 Munich, Germany. Email: roger.smith@lmu.de

The recent study of the sensitivity of tropical-cyclone intensification to the surface drag coefficient in a three-dimensional model by Montgomery *et al.* is extended to include a wind-speed dependent drag coefficient and one of four boundary-layer parameterization schemes: the bulk, Blackadar, MRF and Gayno-Seaman schemes. The schemes are slightly modified to have the same drag coefficient formulation and the same constant exchange coefficients for sensible heat and moisture. Interest is focussed on the change in intensity of the azimuthally-averaged tangential wind speed and change in the low-level vortex structure when the standard value of the drag coefficient is halved or doubled. Changing the drag coefficient provides insight into unbalanced effects in the boundary layer and their impact on the vortex evolution and structure. The changes in vortex behaviour with changing drag coefficient are qualitatively similar for all schemes, the maximum intensification occurring for the standard value of drag coefficient. The interpretation given to explain this behaviour underlines the intrinsically unbalanced nature of the boundary layer dynamics, although, for reasons discussed, a complete theory for the behaviour does not exist. The behaviour found is at odds with the predictions of Emanuel's (balance) theory for the maximum intensity of a tropical cyclone, which predicts a monotonic decrease in intensity with the drag coefficient if the enthalpy exchange coefficient is held fixed. It is at odds also with a recent numerical study of the maximum intensity by Bryan and Rotunno.

The study underscores the importance of boundary-layer dynamics in models for forecasting tropical-cyclone intensity and the need for care in choosing a boundary-layer scheme. However, it is not yet known which boundary-layer formulation is the most appropriate for this purpose, highlighting the need for a concerted research effort in this direction.

Key Words: Hurricanes; tropical cyclones; typhoons; surface drag coefficient; frictional drag

Received June 16, 2010; Revised October 20, 2011; Accepted

Citation: . . .

1. Introduction

A tropical cyclone can be viewed as a complex heat engine that extracts heat energy from the sea surface, mainly in the form of latent heat, and radiates sensible heat to space in the upper troposphere (Kleinschmidt 1951, Emanuel 2004 and refs.). It loses mechanical energy primarily in the form of frictional drag at the ocean surface and does work in creating an upper-level anticyclone. Angular momentum associated with the background rotation of the

Report Documentation Page

Form Approved
OMB No. 0704-0188

1. REPORT DATE	2. REPORT TYPE	3. DATES COVERED
OCT 2011		**00-00-2011 to 00-00-2011**

4. TITLE AND SUBTITLE	5a. CONTRACT NUMBER
Sensitivity of tropical cyclone models to the surface drag coefficient in different boundary-layer schemes	5b. GRANT NUMBER
	5c. PROGRAM ELEMENT NUMBER
6. AUTHOR(S)	5d. PROJECT NUMBER
	5e. TASK NUMBER
	5f. WORK UNIT NUMBER
7. PERFORMING ORGANIZATION NAME(S) AND ADDRESS(ES) **Naval Postgraduate School,Department of Meteorology,Monterey,CA,93943**	8. PERFORMING ORGANIZATION REPORT NUMBER
9. SPONSORING/MONITORING AGENCY NAME(S) AND ADDRESS(ES)	10. SPONSOR/MONITOR'S ACRONYM(S)
	11. SPONSOR/MONITOR'S REPORT NUMBER(S)

12. DISTRIBUTION/AVAILABILITY STATEMENT
Approved for public release; distribution unlimited

13. SUPPLEMENTARY NOTES

14. ABSTRACT

15. SUBJECT TERMS

16. SECURITY CLASSIFICATION OF:			17. LIMITATION OF ABSTRACT	18. NUMBER OF PAGES	19a. NAME OF RESPONSIBLE PERSON
a. REPORT **unclassified**	b. ABSTRACT **unclassified**	c. THIS PAGE **unclassified**	**Same as Report (SAR)**	**13**	

earth is drawn into the cyclone by an overturning circulation brought about by the collective effect of buoyancy in deep rotating clouds. A fraction of the angular momentum drawn inwards is lost because of the frictional torque at the sea surface.

Recent research using three-dimensional numerical simulations has shown that the spin up of intense winds in the inner core of the cyclone actually occurs within a shallow friction layer, or boundary layer, near the sea surface, which is approximately 500 m deep (Zhang *et al.* 2001, Smith *et al.* 2009, Bui *et al.* 2009). The simulations indicate that the spin up is strongly controlled by dynamical processes in the boundary layer and that spin up in models may be sensitive not only to the representation of surface drag, but also to the representation of vertical turbulent mixing of momentum in the boundary layer. To obtain a more complete understanding of these sensitivities requires idealized modelling studies designed to isolate as far as possible the basic physical processes involved. In this spirit, Montgomery *et al.* (2010) re-examined the sensitivity of tropical-cyclones in a three-dimensional, non-hydrostatic, cloud-representing numerical model to the surface exchange coefficient of momentum and Smith and Thomsen (2010) examined the sensitivity to the choice of the boundary-layer parameterization with the same exchange coefficients.

Early theoretical and numerical studies of the sensitivity to the surface exchange coefficients in axisymmetric models found that the intensity decreases markedly with increasing drag coefficient (Emanuel 1995, Craig and Gray 1996 and refs.). In contrast, Montgomery *et al.* (2010) found that, in a three-dimensional model, the intensification rate and maximum intensity of the vortex *increase* with increasing surface drag coefficient until a certain threshold value is attained and then decrease. Moreover, whereas a vortex intensifies in the Emanuel and Rotunno (1987) axisymmetric model when there is no surface drag, no system-scale intensification occurs in the three-dimensional model used, despite persistent sea-to-air fluxes of moisture that maintain deep convective activity. The Montgomery *et al.* (2010) calculations were carried out using the Pennsylvania State University-National Center for Atmospheric Research fifth-generation Mesoscale Model (MM5) with the bulk aerodynamic boundary-layer parameterization and *constant* (i.e. wind-speed independent) surface exchange coefficients. Deep convection was modelled using a warm-rain scheme and radiation was parameterized crudely using a Newtonian relaxation scheme so as to minimize the generation of excessive convective instability in the vortex environment, where the grid resolution is insufficient to represent convection. The new findings were interpreted using recent insights obtained on tropical-cyclone intensification, which highlight the intrinsically unbalanced dynamics of the tropical-cyclone boundary layer and the three-dimensional nature of the spin up process.

Smith and Thomsen (2010) carried out experiments with a similar version of the MM5 model to investigate the dependence of tropical-cyclone intensification and, in particular, the structure of the tropical-cyclone boundary layer, on the representation of the boundary layer in the model. Predictions using one of five available schemes were compared, not only between themselves, but where possible with recent observational analyses of hurricane boundary-layer structure. These schemes included the bulk aerodynamic scheme, the Blackadar scheme, the Burk-Thompson scheme, the MRF-scheme and the Gayno-Seaman scheme. The surface exchange coefficients in all schemes were modified to reflect recent measurements and they were taken to be the same to facilitate a proper comparison of the schemes. The study showed that there is a significant sensitivity of vortex evolution, specifically to the onset time of rapid intensification, the low-level wind structure in the inner-core region, and to the intensity after five days of integration to the particular boundary-layer scheme used. Some of these differences were traced to the different vertical eddy diffusivities determined by the schemes. In particular, the MRF scheme appears to be overdiffusive compared with the others in the tropical cyclone context, consistent with the finding of Braun and Tao (2000) and also with the few available observational estimates at high wind speeds over the ocean (Zhang *et al.* 2010 and refs.). Nevertheless, in other applications the scheme has been found to be the more skillful (e.g. Thomsen and Smith 2008). The Smith and Thomsen (2010) study fell short of being able to advocate the use of a particular scheme, although certain shortcomings of individual schemes were identified in relation to their ability to capture realistic vertical wind profiles and surface inflow angles. It was pointed out that the current inability to determine "the optimum scheme" has implications for the predictability of tropical-cyclone intensification. Nevertheless, the differences between schemes provide an estimate of forecast uncertainty.

Smith and Thomsen (2010) found that the vertical eddy diffusivity is an important quantity because it determines the local boundary-layer depth and hence the magnitude of the radial force imbalance in the boundary layer. This finding appears to conflict with the conclusion of Bryan and Rotunno (2009a, p1777) that "there is a strong sensitivity to l_h, but essentially no sensitivity to l_v (the vertical mixing length)". They use the horizontal and vertical mixing lengths, l_h and l_v, to assess the dependence of cyclone intensity on the sub-grid scale mixing formulation. One could argue that a lack of sensitivity to l_v implies a lack of sensitivity to the vertical eddy diffusivity. However, one cannot make a one-to-one correspondence between the mixing length and the eddy diffusivity on account of the assumed dependence of the diffusivity not only on the mixing length, but also on the local flow deformation and static stability.

The above discussion highlights the need to further understand the influence of the boundary layer on vortex intensification. Given the efforts that have been devoted to including wind-wave coupling for the intensification problem (Chen *et al.* 2007), it is essential to understand further the intrinsic dependencies of the intensification process on the vertical eddy diffusivity and on the surface drag. In this paper we focus on the second problem and extend the study of Montgomery *et al.* (2010) to include a wind-speed dependent drag coefficient in conjunction with different boundary-layer schemes. This approach permits us to assess the universality of these dependencies. We use the Smith and Thomsen version of MM5 in conjunction with one of four available boundary-layer schemes in the model: the bulk scheme, the Blackadar scheme, the MRF scheme and the Gayno-Seaman scheme.

In section 2 we describe briefly the numerical model. The calculations performed are detailed in section 3 and supporting interpretations of them are presented in section

4. A discussion of the results together with an articulation of some remaining scientific issues is the subject of section 5 and a summary with conclusions is given in section 6.

2. The numerical model

The numerical experiments are similar to those described in Nguyen *et al.* (2008). They are carried out using a modified version of MM5 (version 3.6). The model is configured with three domains: a coarse mesh of 45-km resolution and two, two-way nested domains of 15 and 5 km resolution, respectively. The domains are square and are 9000 km, 4500 km, 1500 km on each side. The calculations are performed on an f-plane centred at 20^0N. In all calculations there are 24 σ-levels in the vertical, 10 of which are below 850 mb (see Smith and Thomsen 2010, section 2.1) and therefore believed adequate for resolving the boundary layer dynamics under the prescribed changes to the surface exchange coefficients and vertical mixing of heat and momentum. There is no representation of dissipative heating.

Deep moist convection is resolved explicitly and represented by the warm-rain scheme as in Montgomery *et al.* (2010). In addition, we choose one of four boundary-layer schemes available in the model as detailed in subsection 2.1 (see also the appendix of Smith and Thomsen 2010). The warm-rain and boundary-layer schemes are applied in all domains. No cumulus parameterization is used. The sea surface temperature is a constant (27^{o}C). In contrast to Montgomery *et al.* (2010), who used Newtonian relaxation to the ambient temperature profile as a radiative damping scheme, we use the simple radiative cooling scheme available in MM5, which imposes a temperature-dependent cooling rate on the order of 1-2^{o}C/day. This choice helps allay some concerns that have been raised recently (Hakim 2011) on the appropriateness of the radiative relaxational scheme that has been used in many idealized tropical cyclone studies (e.g., Rotunno and Emanuel 1987, Persing and Montgomery 2003, Bryan and Rotunno 2009a).

The initial vortex is axisymmetric with a maximum tangential wind speed of 15 m s^{-1} at the surface at a radius of 120 km. The magnitude of the tangential wind decreases sinusoidally with height, vanishing at the top model level. The temperature field is initialised to be in gradient wind balance with the wind field using the method described by Smith (2006). The far-field temperature and humidity are based on Jordan's Caribbean sounding for the hurricane season (Jordan 1958).

For the purpose of calculating azimuthal averages, the vortex centre is defined as the centroid of relative vorticity at 900 mb over a circular region of 200 km radius from a "first-guess" centre, which is determined by the minimum of the total wind speed at 900 mb.

2.1. *The boundary-layer schemes*

The four boundary-layer schemes examined here are listed in Table 1 of Smith and Thomsen (2010) together with a brief description of each. In the four main sets of calculations, the surface drag and heat and moisture exchange coefficients are modified to fit the results of the coupled boundary layer air-sea transfer experiment (CBLAST: see Black *et al.* 2007, Drennan *et al.* 2007, French *et al.* 2007, Zhang *et al.* 2008) to facilitate a proper comparison of the schemes. The surface exchange coefficients for sensible heat and moisture are set to the same constant, 1.2×10^{-3}, and that for momentum, the standard drag coefficient, C_{Do} is set to $0.7 \times 10^{-3} + 1.4 \times 10^{-3}(1 - \exp(-0.055|\mathbf{u}|))$, where $|\mathbf{u}|$ is the wind speed at the lowest model level. This formula provides an acceptable approximation to the data on C_D, which has a lot of scatter. The drag coefficient and the exchange coefficients for heat and moisture were modified indirectly in the Blackadar, MRF and Gayno-Seaman scheme using formulae given in the appendix of Hill and Lackman (2009). In essence, the friction velocity is replaced by $V_o\sqrt{C_D}$, where V_o is the total wind speed at the lowest model level.

3. The calculations

We carried out a series of numerical experiments of vortex intensification based on the canonical thought experiment discussed by Nguyen *et al.* (2008), but using four of the five boundary-layer schemes investigated by Smith and Thomsen (2010). For all four schemes we compare calculations using the standard drag coefficient with those in which the drag coefficient is halved and doubled. In all calculations, the surface exchange coefficients for sensible and latent heat are held constant.

For two of the schemes, we carry out also an ensemble of calculations for some values of the drag coefficient in which the initial moisture field is randomly perturbed with values not exceeding 0.5 gm kg^{-1} in magnitude at altitudes below the 900 mb level (about 1 km). The method follows that of Nguyen *et al.* (2008). The aim is to demonstrate the significance of the differences between calculations when the drag coefficient is halved or doubled. Because of the computational expense, ensemble calculations were carried out only for the Blackadar and Gayno-Seaman schemes where it was felt that they were most necessary.

4. Results

4.1. *Vortex evolution*

Figure 1 shows time series of the maximum azimuthally-averaged tangential velocity component, v_{max}, and maximum azimuthally-averaged radial *inflow* component, u_{min}, for the four sets of calculations described above including the ensembles. The salient points to note are as follows.

For all schemes, both the maximum tangential wind speed and maximum inflow increase steadily with time as the vortex intensifies. Both these quantities show fluctuations that may be attributed to the stochastic nature of the deep vortical convective elements (dubbed 'vortical hot towers' or VHTs) that are the fundamental coherent structures driving the spin-up process (Nguyen *et al.* 2008). The inflow at any given time is appreciably larger with the bulk and Blackadar schemes than with the MRF and Gayno-Seaman schemes.

For all except the Gayno-Seaman scheme, the inflow is larger at most times when the value of the drag coefficient is increased. With the bulk scheme, there are small time intervals when, on account of the flow fluctuations, u_{min} is almost the same in the cases with $C_D = C_{Do}$ and $C_D = 2C_{Do}$. With the Blackadar scheme, the ensemble calculations of u_{min} for $C_D = 2C_{Do}$ are mostly larger than

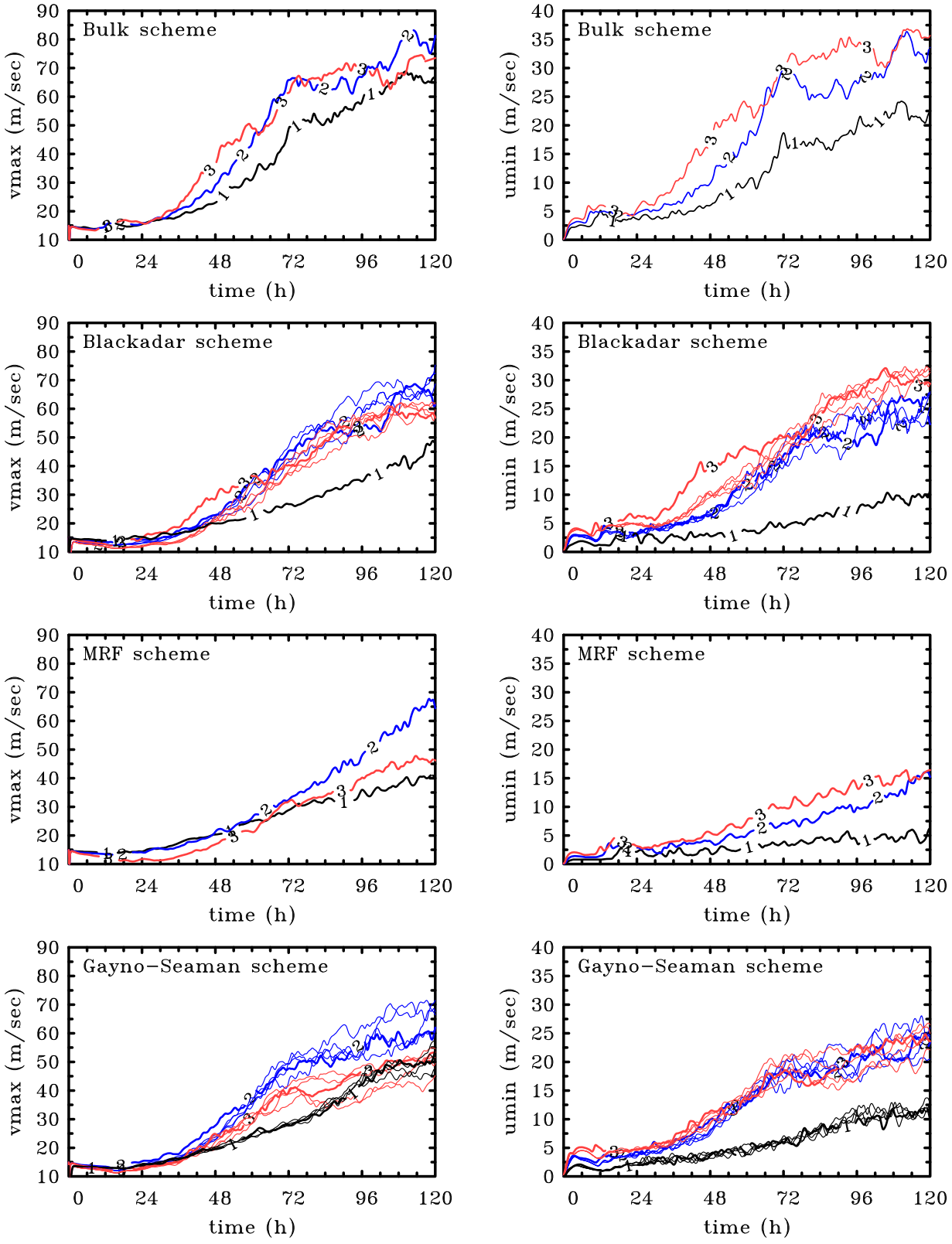

Figure 1. Time-series of maximum azimuthally-averaged tangential wind, v_{max}, (left panels) and maximum azimuthally-averaged radial inflow, u_{min}, (right panels) in the calculations with the bulk scheme (upper panels), the Blackadar scheme (upper middle panels) the MRF scheme (lower middle panels), and the Gayno-Seaman scheme (lower panels). Curves 1 (black): $C_D = \frac{1}{2}C_{Do}$; curves 2 (blue): $C_D = C_{Do}$; and curves 3 (red): $C_D = 2C_{Do}$.

those for $C_D = C_{Do}$, although there is a slight overlap*.

*One of the principle findings of Nguyen *et al.* (2008) was the demonstration that the intensification process and maximum mean tangential wind possesses an intrinsic stochastic element associated with the vortical convective elements. In view of this result, each time series in Figure 1 should be regarded as a single member of an ensemble generated by, say, small moisture variations in the boundary layer. Based on the findings in Nguyen *et al.* (2008), which show a spread on the order of 10 m s^{-1} in the maximum azimuthally-averaged tangential velocity amongst ensemble members during the intensification phase, the

With the MRF scheme, the differences in u_{min} between $C_D = C_{Do}$ and $C_D = 2C_{Do}$ are clear for much of the calculation time, but they are not large and probably not too significant. With the Gayno-Seaman scheme, there is a clear distinction between the curves for $C_D = \frac{1}{2}C_{Do}$ and $C_D = C_{Do}$ whereas there is a general overlap of curves in the two sets of ensembles for $C_D = C_{Do}$ and $C_D = 2C_{Do}$, suggesting that the differences indicated by the two control runs are not significant. Note also that the spread of the ensembles for the Gayno-Seaman scheme with $C_D = \frac{1}{2}C_{Do}$ is comparatively small.

The increase of the inflow with increasing C_D might be anticipated, even if there were no change in the distribution of latent heat release in the vortex aloft. The reason is that increased drag leads to a greater reduction of the near-surface tangential wind speed, at least in the outer region of the vortex where there is subsidence into the boundary layer. This greater reduction leads to a larger disruption of gradient wind balance and a correspondingly larger inward agradient force (Smith and Vogl 2008, Smith *et al.* 2009, Montgomery *et al.* 2010). The assumption is that this larger force is not outweighed by an increase in the frictional force in the radial direction. Of course, in the calculations here, the coupling between the vortex aloft and the boundary layer means that changes in the vortex on account of changes in the pattern of latent heat release may explain some of the changes in the calculated behaviour. Such changes would be expected to be associated mostly with changes in the moisture distribution in the boundary layer (see section 5).

In contrast to the behaviour of u_{min}, v_{max} first increases as C_D is increased from $\frac{1}{2}C_{Do}$ to C_{Do} and then decreases, or remains more or less the same, as C_D is increased further to $2C_{Do}$. The reason, in part, is that the increased boundary-layer inflow brings air parcels closer to the vortex centre leading to the tendency for them to spin faster due to the partial conservation of absolute angular momentum[†]. This tendency is offset by the frictional torque, which reduces the absolute angular momentum. If on account of an increase in C_D, air parcels converge sufficiently rapidly, the loss of absolute angular momentum may be more than offset by the radial displacement towards the centre leading to a higher tangential wind speed maximum (Smith and Vogl 2008, Smith *et al.* 2009, Montgomery *et al.* 2010). Figure 1 shows that the circumstances when the convergence of absolute angular momentum dominates is in the lower range of drag coefficients studied: between $\frac{1}{2}C_{Do}$ and C_{Do}. However, as C_D is increased further, the increased torque wins. Thus, all schemes have an optimum drag for the maximum intensification of v_{max}. This result is to be expected from the results of Montgomery *et al.* (2010), since the case of zero drag gives no sustained intensification and the case of extreme drag gives little intensification also.

The foregoing results are especially significant in the light of Emanuel's theory for the potential intensity of a tropical cyclone (Emanuel 1986, Emanuel 1995, Bister and Emanuel 1998), which predicts a decrease in v_{max} as the drag coefficient increases (see e.g. Emanuel 1995, Figure 1). Although the calculations of Bryan and Rotunno (2009a) and the preferred parameter settings therein largely support these theoretical predictions (see their Figure 6), we do not understand their findings and attribute the discrepancy to an inadequate representation of the boundary layer, or the use of an axisymmetric model. The three-dimensional calculations here and in Montgomery *et al.* (2010) do not exhibit such behaviour as the drag coefficient is varied. Contrary to a prediction of Emanuel's (1995) theory, there is an optimum value of C_k/C_D for maximum intensification.

4.2. *Low-level wind structure*

Figure 2 shows radius-height cross-sections of the azimuthally-averaged radial velocity component, u, and tangential velocity component, v, in the lowest 3 km, averaged during the period 114-120 hours, for the calculations with the Blackadar and MRF-schemes. The three panels for each scheme show fields for $C_D = \frac{1}{2}C_{Do}$, C_{Do}, and $2C_{Do}$. Prominent features are that v_{max} occurs at low levels near the top of the frictionally-induced inflow layer in all cases, while u_{min} occurs very close to the surface, in accord with the findings of Smith *et al.* (2009). However there are significant differences in the behaviour of the two schemes to increasing C_D as follows.

4.2.1. *Blackadar scheme*

With the Blackadar scheme, the radius of v_{max} decreases significantly as the C_D increases, being about 80 km for $C_D = \frac{1}{2}C_{Do}$, 40 km for $C_D = C_{Do}$, and 33 km for $C_D = 2C_{Do}$. The radius of u_{min} decreases also as C_D is increased. A physical explanation for this behaviour follows directly from the ideas discussed in the previous section. The increased friction leads to a larger gradient wind imbalance in the boundary layer. With the higher C_D value, inflowing rings of boundary layer air are subjected to a greater agradient force and hence are driven farther inwards before rising out of the boundary layer and ascending into the eyewall updraught. The end result is an enhanced maximum tangential wind, despite some loss of absolute angular momentum en route (see Nguyen *et al.* 2002, Smith *et al.* 2009 and Montgomery *et al.* 2010).

The foregoing argument assumes that the boundary-layer depth, as characterized by the depth of appreciable inflow [‡], remains essentially unaltered as the drag coefficient changes. However, as noted by Smith and Vogl (2008), the effects of surface drag are distributed through the depth of the boundary layer and a change in the depth through which the net radial force acts will change the strength of the inflow. As seen in Figure 2, the depth of the inflow increases with increasing drag, but only marginally as C_D goes from C_{Do} to $2C_{Do}$. This behaviour is consistent with

differences between runs that are less than this amount would not be regarded as significant.

[†]The absolute angular momentum, M, is defined by $rv + \frac{1}{2}fr^2$, where r is the radius, v is the tangential wind component and f is the Coriolis parameter. Near the surface, M is not conserved on account of the frictional torque. Nevertheless, the convergence of M leads to spin-up if air parcels can be brought to small radii quickly enough, before losing an appreciable amount of M (Smith and Vogl 2008, Smith *et al.* 2009).

[‡]Following Smith *et al.* (2009), we use the term *boundary layer* to describe the shallow layer of *strong* inflow near the sea surface that is typically 500 m to 1 km deep and which arises *largely* because of the frictional disruption of gradient wind balance near the surface. Although there is some inflow throughout the lower troposphere associated with the balanced response of the vortex to latent heat release in the eyewall clouds (Bui *et al.* 2009), the largest radial wind speeds are confined within the lowest kilometre and delineate clearly the layer in which friction effects are important (i.e. where there is gradient wind imbalance: see Figure 6 of Smith *et al.* (2009).) from the region above where they are not.

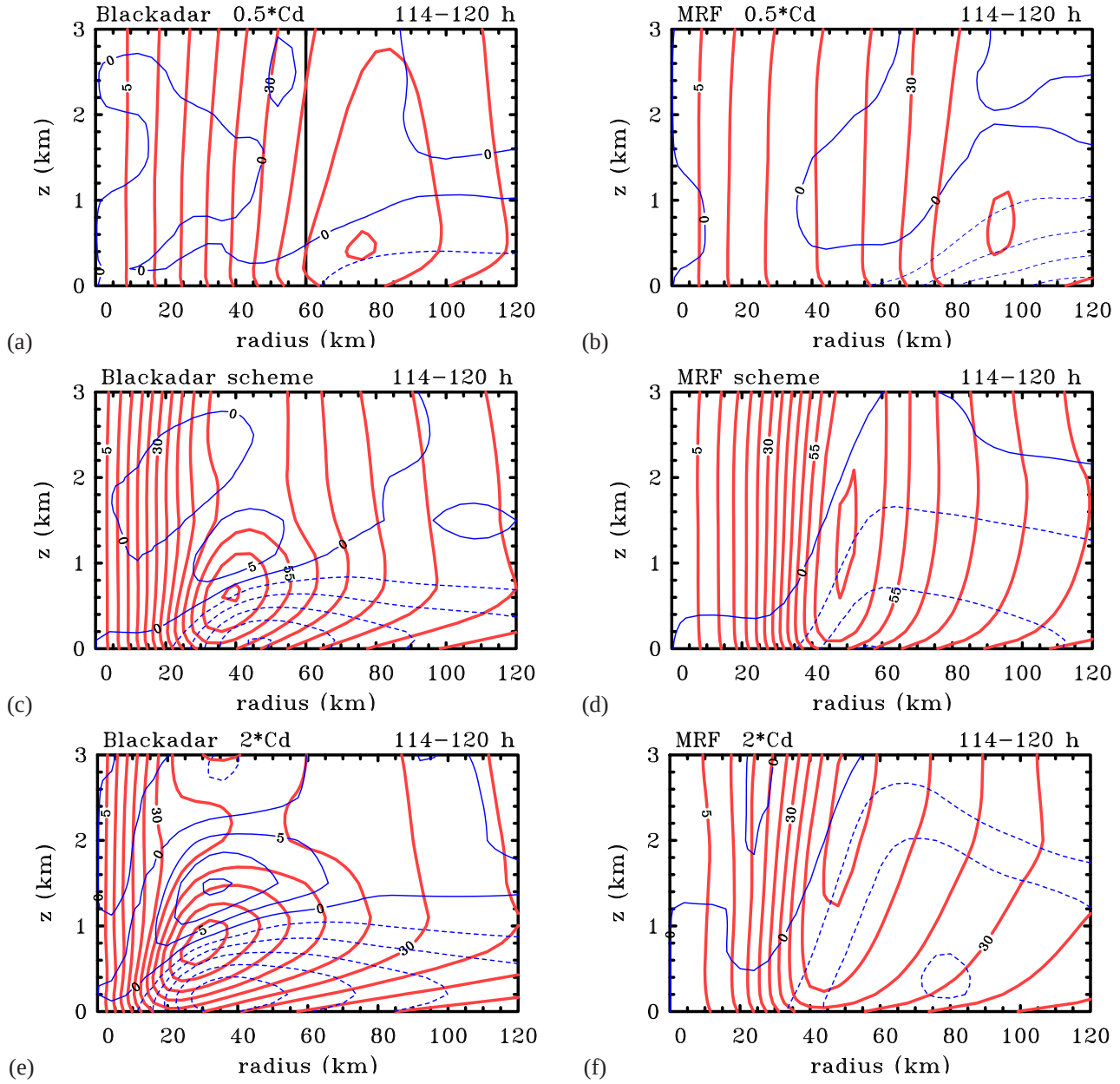

Figure 2. Radius-height cross-sections of azimuthally-averaged radial (thin/blue lines) and tangential (thick/red lines) wind speed components in the lowest 3 km averaged over the period 114-120 hours for the Blackadar scheme (left panels) and MRF scheme (right panels). The contours of the tangential component are the thick (and red) solid lines; those of the radial component are thin and blue lines with negative values dashed. (a),(b) $C_D = \frac{1}{2}C_{Do}$, (c),(d) $C_D = C_{Do}$, and (e),(f) $C_D = 2C_{Do}$. Contour interval 5 m s^{-1} for both components, *except for the radial component in panel (b)*, where it is only 1 m s^{-1}.

the predictions of linear theory, which shows that the height of maximum inflow generally increases with increasing C_D (Kepert, 2001, Fig 1).

Vogl and Smith (2009) presented a scale analysis of the boundary layer showing that the boundary-layer depth is proportional to the square root of the eddy diffusivity. While the eddy diffusivity is assumed constant in that analysis, in more general situations the boundary-layer depth may be assumed to increase with some vertical average of the eddy diffusivity. The distribution of eddy diffusivity predicted by the various schemes is discussed further in section 4.3.

4.2.2. MRF scheme

With the MRF scheme, the layer of appreciable inflow is much deeper than with the Blackadar scheme, a result that is consistent with the relatively large eddy diffusivity in this scheme. We show in section 4.3 that the eddy diffusivities predicted by the MRF scheme are much larger than for the Blackadar scheme for the same representation of drag coefficient. There is again a relatively large change in the radius of v_{max} as C_D goes from $\frac{1}{2}C_{Do}$ to C_{Do}, but little change as it goes from C_{Do} to $2C_{Do}$. Moreover, as for the Blackadar scheme, the radius of u_{min} decreases as C_D goes from $\frac{1}{2}C_{Do}$ to C_{Do}, but unlike the behaviour with the Blackadar scheme, it increases as C_D goes from C_{Do} to $2C_{Do}$. It follows that for an increase in drag coefficient beyond the standard value in the MRF scheme, the tangential wind tendency accompanying the increased convergence of absolute angular momentum is much more than compensated by the negative tendency of friction. The weaker inflow with the MRF scheme has interesting

consequences for the pattern of vertical motion as discussed in section 5.4.

4.2.3. *Other schemes*

For space reasons we have not shown figures corresponding to Figure 2 for the other two schemes, but simply summarize the results. The changes in low-level structure with the change in drag coefficient in the case of the bulk scheme is similar to that of the Blackadar scheme, but the vortex in the case with $C_D = \frac{1}{2}C_{Do}$ is more intense than its counterpart with the Blackadar scheme (compare panels (a) and (c) of Figure 2). The behaviour in the case of the Gayno-Seaman scheme is similar to that with the Blackadar scheme in that the vortex in the 114-120 hour average with $C_D = \frac{1}{2}C_{Do}$ is considerably weaker than those for C_D and $C_D = 2C_{Do}$. However, the vortex for $C_D = 2C_{Do}$ is only slightly weaker than that for $C_D = C_{Do}$.

4.3. *Eddy diffusivity*

Some of the differences in behaviour between schemes can be interpreted in terms of the distribution of vertical eddy diffusivity that they deliver. While the schemes investigated have various degrees of sophistication, almost all seek to determine some local value of turbulent diffusivity, $K(r, z)$, to close the momentum and thermodynamic equations. An exception is the Blackadar scheme in the (dry) convective regime, which uses a non-local mixing algorithm. In our calculations, we found that this algorithm is not invoked within 200 km of the centre of the vortex circulation. In other stability regimes of this scheme, the formulation for $K(r, z)$ is exactly the same as in the Bulk scheme. In both these schemes, K is the product of the square of a mixing length, the vertical wind shear, and a specified function of the Richardson number (see Blackadar 1976). In the MRF scheme, the determination of K is based on empirical formulae while in the Gayno-Seaman scheme it is related to the turbulent kinetic energy, which is a prognostic quantity in this scheme.

Figure 3 shows radius-height cross-sections of the vertical eddy diffusivity in the lowest 3 km, averaged during the period 114-120 hours, for the calculations with the Blackadar and MRF-schemes for $C_D = \frac{1}{2}C_{Do}$, C_{Do} and $2C_{Do}$. The patterns in all four schemes including the two not shown are similar. In particular, there is a low-level maximum of K in the region of maximum tangential wind speed as well as elevated values in the eyewall updraught. The main updraught is indicated in the figure by the 0.2 m s^{-1} contour of vertical velocity (0.1 m s^{-1} contour in panel (b)). There is a strong radial gradient of K also and, for the two schemes in the figure, the values of K increase with increasing drag coefficient.

Maximum values of K for all the schemes are shown as time series in Figure 4, where it is seen that the MRF scheme is by far the most diffusive with a maximum of nearly 600 m^2 s^{-1} (note the 5-fold increase in contour interval needed for this scheme). This result explains why the inflow layer is much deeper in the MRF scheme and, because the surface drag is therefore distributed over a much deeper layer, why the local disruption of gradient balance is smaller leading to a substantially weaker inflow.

Maximum values of K with the bulk scheme are comparable with, but systematically a little larger than those with the Blackadar scheme and lie in the range 60-120 m^2 s^{-1}. In contrast, the Gayno-Seaman scheme is relatively diffusive with maxima values of K reaching about 250 m^2 s^{-1}. All schemes except the Gayno-Seaman scheme predict a marked increase in the maximum K as the drag coefficient is increased. With the Gayno-Seaman scheme, the maximum K changes relatively little, although there are noticeable differences in the *distribution* of K when the drag coefficient is increased (not shown). For example, the areal extent within the $K = 50$ m^2 s^{-1} contour in the azimuthal-mean, radial-height cross section increases significantly, but not as much as with the MRF scheme.

The only observational estimates for K that we are aware of are those analysed recently from flight-level wind measurements at an altitude of about 500 m in Hurricanes Allen (1980) and Hugo (1989) by Zhang *et al.* (2010). In Hugo these were about 110 m^2 s^{-1} beneath the eyewall, where the near-surface wind speeds were about 60 m s^{-1}, and in Allen they were up to 74 m^2 s^{-1}, where wind speeds were about 72 m s^{-1} (Zhang *et al.* 2010). One might be tempted to judge that the MRF and Gayno-Seaman schemes are much too diffusive, whereas the other schemes have broadly realistic diffusivities, but it would be premature to draw firm conclusions from a comparison with only two observational estimates!

5. Discussion and some remaining scientific issues

The interpretations given above for the vortex behaviour as a result of changing the boundary-layer scheme, or changing the drag coefficient within a scheme, go some way to providing basic understanding of the problem. However, they fall short of providing a complete theory, which would entail the construction of a physically-consistent model to mimic the behaviour shown. So far, the interpretations have focussed on boundary layer processes, but a complete theory would require consideration of processes above the boundary layer as well. Even though the enthalpy exchange coefficients are held constant in all calculations, a change in the surface wind speed brought about by a change in the value of C_D will lead to a change in the surface enthalpy flux, unless the air-sea disequilibrium were to exactly compensate. The latter scenario is highly improbable. A change in enthalpy fluxes (primarily latent heat) must feed back to affect the spatial distribution of diabatic heating and the aggregate affects of buoyancy associated with deep convection. At this stage we are unaware of a satisfactory theory to link these changes with a change in C_D. The most we can do here is to attempt to articulate the main challenges in developing such a theory.

First we note that the interpretations given herein are based on axisymmetric reasoning. While the flow asymmetries in the form of rotating deep convective clouds [§] are quantitatively important in the flow dynamics, it is their collective effect which is relevant to the present discussion, so that axisymmetric reasoning should suffice.

5.1. *The intensification stage*

We consider first the intensification stage. As shown in Bui *et al.* (2009), the convective clouds provide an aggregate heating rate that drives a system-scale convergence of

[§] An examination of the vertical motion fields at the 850 mb level shows that the character of the convection does not change in any obvious way with a change in boundary-layer scheme.

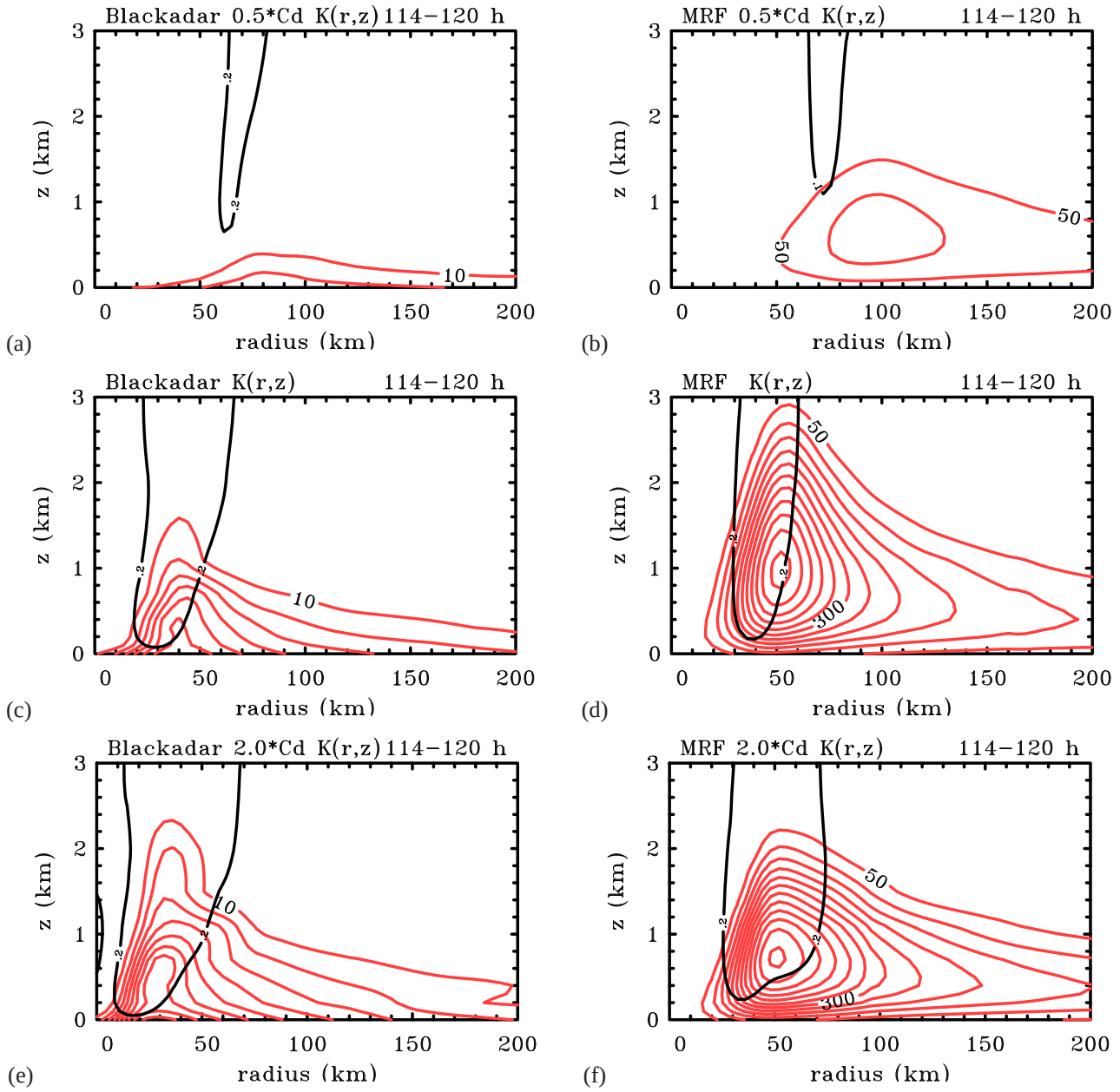

Figure 3. Radius-height cross-section of the time-mean, azimuthally-averaged eddy diffusivity, $K(r, z)$, during the period 114-120 hours for the Blackadar scheme (left panels, contour interval 10 m^2 s^{-1}) and MRF scheme (right panels, contour interval 50 m^2 s^{-1}). (a),(b) $C_D = \frac{1}{2}\times$ standard; (c),(d) C_D = standard; (e)(f) $C_D = 2\times$ standard. The main updraught is indicated in the figure by the thick black contour, which depicts the 0.2 m s^{-1} contour of the same time-mean azimuthally-averaged vertical velocity, *except in panel (b)* where the contour value is 0.1 m s^{-1}.

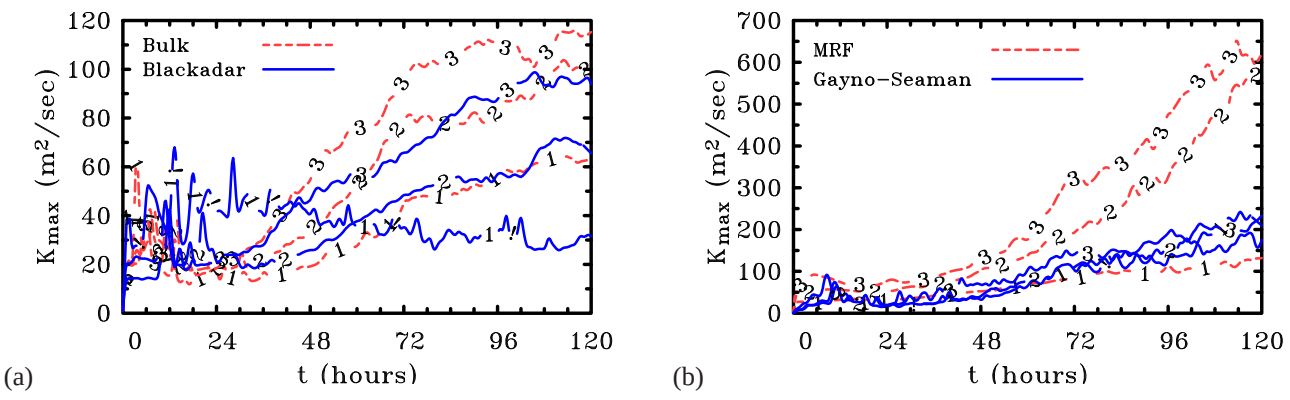

Figure 4. Time-series of maximum azimuthally-averaged eddy diffusivity, K_{max}, for the four modified boundary-layer schemes: (a) bulk (red) and Blackadar (blue) schemes; and (b) MRF (red) and Gayno-Seaman (blue) schemes. Curves 1 refers to $C_D = \frac{1}{2}C_{Do}$, curves 3 to $C_D = C_{Do}$, and curves 4 to $C_D = C_{Do}$. *Note the different scales along the ordinate in the two panels.*

absolute angular momentum *above* the boundary layer, where this quantity is approximately materially conserved. The net effect of this convergence is to spin up the circulation there. The situation in the boundary layer is more subtle. We would argue that the vortex-scale inflow in the boundary-layer is a response to the azimuthally-averaged tangential wind at the top of the boundary layer and, because of the parabolic nature of the boundary-layer equations, convection cannot "suck" inflow in the boundary-layer, except possibly near to convection where boundary-layer theory breaks down. As noted earlier, the inflow in the boundary layer is much stronger than that above on account of the inwards-directed agradient force, but absolute angular momentum in this layer is lost by the frictional torque. Typically, in the inner-core region, the tangential wind becomes supergradient and, as a result, the maximum tangential wind speed occurs within, but near the top of the boundary layer.

The diabatic heating rate associated with deep convection depends on both the vertical velocity and specific entropy of ascending air, the radial distribution of which must be determined by the boundary layer dynamics and thermodynamics. The boundary-layer dynamics must determine also the radial distribution of horizontal momentum (including angular momentum) of the ascending air following its spin up in the boundary layer. Above the boundary layer, a scale analysis indicates that the flow is close to gradient wind balance (Willoughby 1979), so that the secondary circulation is governed there by the Sawyer-Eliassen equation (Shapiro and Willoughby 1982, Bui *et al.* (2009)), at least during periods of intensity change (see below). In the absence of friction, the forcing term in this equation is primarily the radial gradient of diabatic heating. However, there is an additional forcing at the lower boundary (i.e. the top of the frictional boundary layer) on account of air being expelled from or drawn into the boundary layer.

5.2. *The mature stage*

We consider now the mature stage of development. In a strict steady state, the steps taken to derive the Sawyer-Eliassen equation become degenerate because the time tendencies that are eliminated in the derivation are identically zero. Then, in the absence of friction and/or eddy fluxes of tangential momentum and moist entropy, the azimuthally-averaged secondary circulation above the boundary layer must be along absolute angular momentum surfaces and along moist isentropic surfaces, i.e., these two sets of surfaces must be congruent. However, these constraints are not sufficient by themselves to determine the flow, even if the flow is in balance[¶]. Indeed, as discussed in the footnote below, it is unclear that a steady solution of even the balance problem exists globally. This issue presents a vexing problem in relating the change in diabatic heating distribution with a change in the drag coefficient in the mature stage.

Two further problems of constructing a steady-state theory for a hurricane are the fact that the inner-core boundary layer is not in gradient-wind balance and the top of the boundary layer is open. At radii where there is ascent out of the boundary layer, an open boundary condition is required to allow, *inter alia*, the high tangential wind speeds that are spun up in the boundary layer to be lofted into the interior flow. The formulation of such a condition is problematic as discussed by Smith and Montgomery (2010) and it seems wrong to us to constrain the flow to return to a *prescribed* gradient wind as is typically assumed in steady boundary-layer theory. Because of the tight coupling between the boundary layer and the interior flow, we would be uncomfortable about investigating the effects of changing the drag coefficient by focussing only on the steady boundary layer response and believe that it is essential to solve for the vortex flow as a whole.

5.3. *Effects of changing C_D on the primary circulation*

Notwithstanding the foregoing issues, it may be of interest to the reader to see the differences in the flow above the boundary layer as a result of changes in the drag coefficient. For this reason, we show in Figures 5 and 6 some details of the flow above the boundary layer for the four boundary-layer schemes. We show these figures to provide a context for future theoretical investigations, but at this time we are unable to provide a satisfactory interpretation for the range of behaviour surveyed. Figure 5 shows radial profiles of azimuthally-averaged tangential wind speed, V_g, at a height of 2 km for the four schemes considered and for the three values of drag coefficient for each scheme. The wind speed V_g should be a reasonable approximation to the gradient wind at the top of the boundary layer, but not to the total surface wind, which is one factor determining the latent heat flux.

A common feature of all the schemes is that, like v_{max}, the maximum value of V_g, $V_{g_{max}}$, is largest for $C_D = C_{Do}$. However, unlike v_{max} (cf. Figure 1), for the bulk, Blackadar and Gayno-Seaman schemes, $V_{g_{max}}$ is larger for $C_D = \frac{1}{2}C_{Do}$ than for $C_D = 2C_{Do}$. The exception is the MRF scheme, where $V_{g_{max}}$ is smallest for $C_D = \frac{1}{2}C_{Do}$. The radius of maximum V_g, say r_{Vgmax} varies also with C_D. With the Blackadar and MRF schemes, r_{Vgmax} is about twice as large for $C_D = \frac{1}{2}C_{Do}$ as with $C_D = C_{Do}$, but the difference is less for the bulk scheme and much less for the Gayno-Seaman scheme. With all except the bulk scheme, r_{Vgmax} decreases monotonically with increasing C_D, but the radial profile of V_g with the bulk scheme with $C_D = 2C_{Do}$ is rather flat.

5.4. *Effects of changing C_D on the secondary circulation*

A feel for the differences in the secondary circulation as C_D is halved or doubled is provided by vertical cross sections of

[¶]A more strict constraint on steady balance flow may be obtained from the geopotential tendency equation derived by Shapiro and Montgomery (1993) and Vigh and Schubert (2009). If the flow is symmetrically stable this second-order linear partial differential equation is elliptic with a forcing term that is proportional to the product of potential vorticity, P, with the θ derivative of $\dot{\theta}/P$ along an absolute momentum surface, where θ is the potential temperature and $\dot{\theta}$ is its material derivative. Vigh and Schubert refer to this product as the *cyclogenesis function*. Unlike the Sawyer-Eliassen equation, the derivation of the geopotential tendency equation is not degenerate for steady flow, implying that for such a flow, the cyclogenesis function must be identically zero. This condition determines the secondary circulation in terms of the primary circulation and the diabatic heating (and, in general, other forcing terms), and although the requirement of continuity imposed a further constraint, it does not allow for solution for the primary circulation and mass field. Indeed, it is even unclear that a global steady-state solution exists.

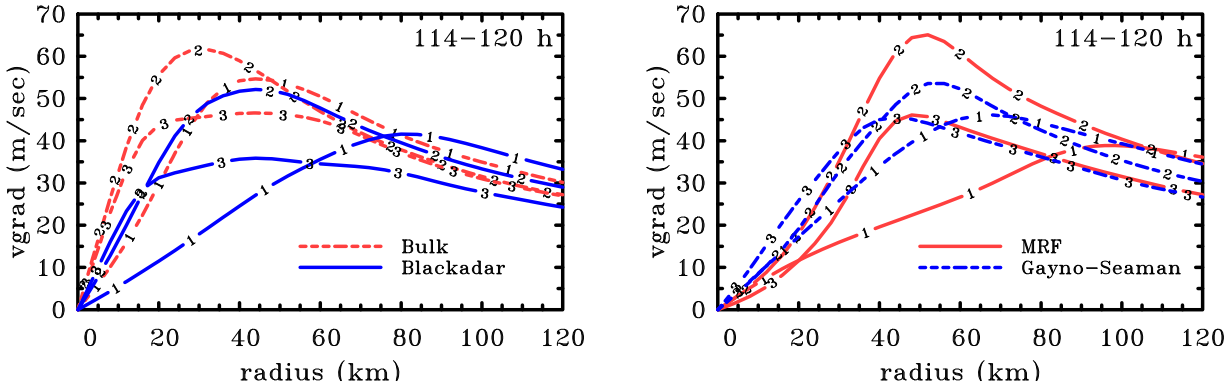

Figure 5. Radial profiles of time-mean azimuthally-averaged tangential wind speed at a height of 2 km (upper panels) for the Bulk and Blackadar schemes (left panels) and the MRF and Gayno-Seaman schemes (right panels) during the period 114-120 hours. Curves 1,2,3 refer to runs with: $C_D = \frac{1}{2}\times$ standard; C_D standard; and $C_D = 2\times$ standard, respectively.

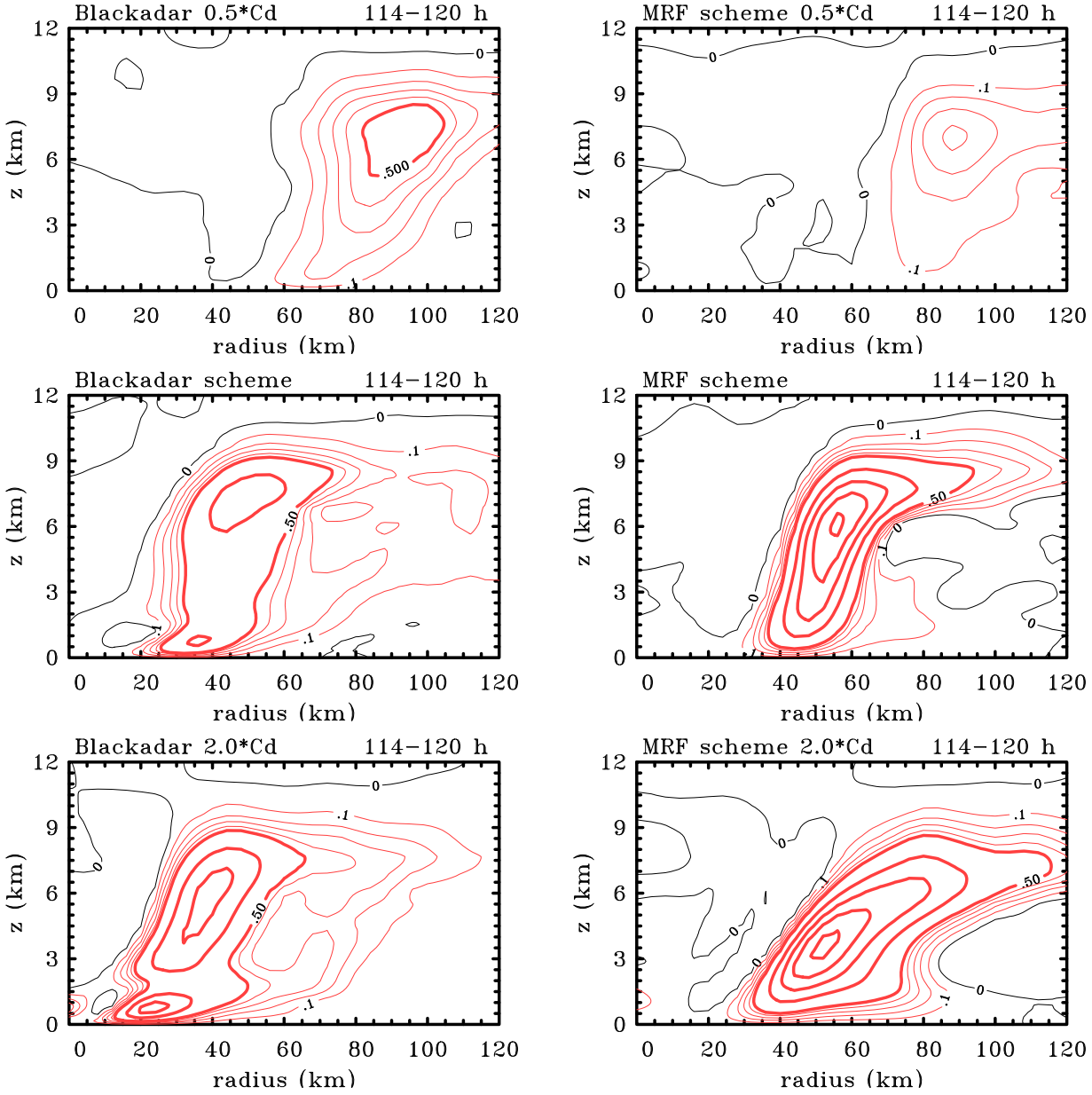

Figure 6. Radius-height cross sections of azimuthally-averaged vertical velocity for the Blackadar scheme (left panels) and MRF scheme (right panels) time averaged between 114 and 120 hours. Contour interval: thick contours 0.5 m s^{-1}; thin contours 0, 0.1, 0.2.0.3 and 0.4 m s^{-1}.) Upper panels: $C_D = \frac{1}{2}\times$ standard; middle panels: C_D standard; and lower panels: $C_D = 2\times$ standard.

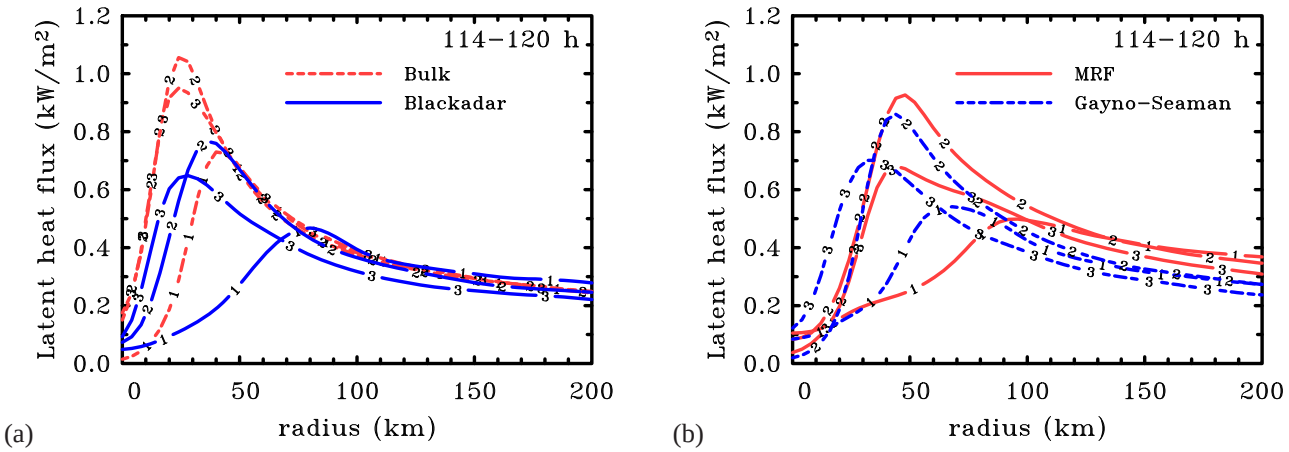

Figure 7. Radial profiles of time-mean azimuthally-averaged latent heat flux for (a) the Bulk and Blackadar schemes, and (b) the MRF and Gayno-Seaman schemes during the period 114-120 hours. Curves 1,2,3 refer to runs with: $C_D = \frac{1}{2}\times$ standard; C_D standard; and $C_D = 2\times$ standard, respectively.

the azimuthally-averaged vertical velocity for the Blackadar and MRF schemes, shown in Figure 6. For both schemes, the mean updraught that marks the time-averaged ascent in the eyewall increases significantly in strength as C_D increases from $\frac{1}{2}C_{Do}$ to C_{Do}. The radius of the maximum updraught contracts inwards also. For the Blackadar scheme the updraught strength increases further as C_D is increased to $2C_{Do}$ and there is a further contraction in radius. A striking feature of this scheme for the two larger values of C_D is the pronounced low-level maximum that is a consequence of the rapid deceleration of the boundary-layer inflow and its eruption into the updraught. This eruption corresponds with a separation of the boundary layer brought about by inertial forces as the tangential wind component becomes supergradient (see e.g. Smith *et al.* 2009, Smith and Montgomery 2010). Subsequent to this eruption, the updraught decelerates on account of the static stability until cloud buoyancy becomes sufficient to re-accelerate it. For the MRF scheme, the vertical velocity field changes more in pattern than in strength as C_D is increased to $2C_{Do}$ and there is little radial contraction. Notably the maximum vertical velocity is lowered and there is no low-level maximum as in the Blackadar scheme. We attribute the absence of the low-level maximum with this scheme to the much higher vertical diffusivity of the scheme, which tends to mitigate the inertial dynamics of the boundary layer.

5.5. *Effects of changing C_D on the surface fluxes*

It has been long recognized that the latent heat supplied by the ocean is the primary energy source for a tropical cyclone (e.g. Riehl 1954). For this reason, theories for tropical cyclone behaviour have laid great emphasis on incorporating these fluxes in the physical formulation. A widely accepted paradigm for tropical cyclone intensification is based on the supposed feedback between the surface wind speed and the latent heat flux (Rotunno and Emanuel 1987). While this feedback process has been called into question recently, it remains true that modest sea-to-air vapour fluxes are essential for supplying buoyancy to rotating deep convection (see Montgomery *et al.* 2009). With this background we show here the effect of changing the drag coefficient on the radial profiles of azimuthally-averaged latent heat flux in the mature stage of the calculation.

Figure 7 shows radial profiles of azimuthally-averaged latent heat flux at the ocean surface in the mature stage. These profiles exhibit a similar behaviour for all schemes as C_D is increased, with the maximum flux occurring when $C_D = C_{Do}$ and the minimum when $C_D = \frac{1}{2}C_{Do}$. This behaviour mirrors that of v_{max}, but not that of V_g, because the latter, in particular, does not characterize the profile of *total* surface wind, and even if it did, the flux depends also on the thermodynamic disequilibrium across the sea surface. The radius of the maximum flux generally decreases with increasing C_D, which is presumably, in part, a reflection of the contraction of the maximum in both wind speed components near the surface (not shown).

At this stage it does not seem possible to give a complete interpretation of the changes in the latent heat flux with the changes in C_D, although the results suggest that the fluxes are largely slaved to the boundary-layer dynamics through the distribution of surface wind speed. A missing link in providing a complete theory is knowing how to relate the surface fluxes to local cloud buoyancy, that, in an aggregate sense is necessary to drive a deep overturning circulation.

6. Summary and conclusions

We have carried out idealized three-dimensional numerical simulations to investigate the sensitivity of tropical-cyclone intensification to changes in the surface drag coefficient in the prototype intensification problem discussed by Nguyen *et al.* (2008). Changing the drag coefficient provides insight into unbalanced effects in the boundary layer and their impact on the vortex evolution. It provides also further understanding of the intrinsic dependencies of the intensification process on the vertical eddy diffusivity and on the surface drag. Because of the tight coupling between the boundary layer and the interior flow, we have purposely solved the vortex problem as a whole and not just the boundary-layer response to the drag coefficient. The study, which uses the MM5 model, extends that of Montgomery *et al.* (2010) to include a wind-speed dependent drag coefficient in conjunction with four different boundary-layer schemes available in MM5: the bulk scheme, the Blackadar scheme, the MRF scheme and the Gayno-Seaman scheme. To facilitate direct comparison, the schemes were modified slightly to have the same drag

coefficient formulation and the same constant exchange coefficients for sensible heat and moisture.

For a control value of the drag coefficient consistent with recent observations, we have investigated the changes in vortex evolution and mature intensity when this control value is halved or doubled. The intensity is characterized by the maximum azimuthally-averaged tangential wind speed. We find that the change in intensity when the drag coefficient is halved or doubled from its standard value depends on the boundary layer scheme employed. In all schemes, the intensity increases as the drag coefficient is increased from half its standard value to the standard value and then declines as the drag coefficient is doubled from its standard value. Thus the standard drag coefficient is close to an optimum value for maximum intensification. The result for the bulk scheme is slightly different from that reported by Montgomery *et al.* (2010), where the decline in intensity with increasing drag coefficient occurred at a much higher value than twice the standard value. The difference is presumably because here, C_D increases with wind speed before levelling off, whereas in Montgomery *et al.* (2010) its value was held constant for simplicity.

The effects of gradient-wind imbalance are reflected in the strength of the inflow, which in all schemes is larger at most times for larger values of the drag coefficient. However, the increase in going from half the standard drag to standard drag is typically larger than for doubling the drag. In fact, except with the Blackadar scheme, the increase with doubling the drag may not be significant. The larger inflow arises because the increased drag, distributed through the depth of the boundary layer by subgrid-scale turbulent diffusion, leads to a larger inward agradient force in the layer.

In general, from an axisymmetric perspective, with a higher drag coefficient, inflowing rings of boundary layer air are converged farther inwards before rising out of the boundary layer and ascending into the eyewall updraught. The change in the maximum tangential wind speed is the net effect of two competing processes: the increase in tangential wind on account of air parcels moving to smaller radii with partial conservation of absolute angular momentum and the decrease on account of the loss of absolute angular momentum along the trajectory. We have shown that the net effect depends on the boundary-layer scheme used and, in particular, on how diffusive the scheme is in the vertical direction. With the two schemes that have a relatively small vertical turbulent eddy diffusivity, the bulk and Blackadar schemes, the decrease in tangential wind in going from the standard value of drag to twice its value is much less than that with the more diffusive MRF and Gayno-Seaman schemes.

The depth of appreciable inflow is much larger with the MRF scheme than with the other schemes. This result is consistent with the relatively large vertical eddy diffusivity in this scheme, which has a maximum value of nearly 600 $\mathrm{m}^2\ \mathrm{s}^{-1}$. Because the surface drag is distributed over a much deeper layer, the local disruption of gradient wind balance is smaller leading to a substantially weaker inflow than for the other schemes.

Maximum values of vertical eddy diffusivity with the bulk scheme are comparable with, but systematically a little larger than, those with the Blackadar scheme and lie in the range 60-120 $\mathrm{m}^2\ \mathrm{s}^{-1}$. In contrast, the Gayno-Seaman scheme is relatively diffusive with maximum values reaching about 250 $\mathrm{m}^2\ \mathrm{s}^{-1}$. All schemes except the Gayno-Seaman scheme predict a marked increase in the maximum diffusivity as the drag coefficient is increased. This increase might be expected in a boundary layer with mechanically-driven turbulence. The lack of sensitivity of the diffusivity to the drag coefficient in the Gayno-Seaman scheme is interesting, but remains to be investigated.

Despite the fact that the exchange coefficients for heat and moisture are held fixed, the finding that there exists an optimum drag coefficient for maximum intensity is significant in the light of Emanuel's theory for the potential intensity of a tropical cyclone (Emanuel 1995). This theory predicts a *decrease* in intensity with increasing drag coefficient for a fixed enthalpy exchange coefficient. The intrinsically unbalanced dynamics of the boundary layer emphasized here is not a feature of Emanuel's theory (Smith *et al.* 2008 and Smith and Montgomery 2008). The present study underscores the importance of adequately representing the boundary-layer dynamics in models for forecasting tropical-cyclone intensity. However, it is not yet known which boundary-layer formulation is the most appropriate for this purpose, highlighting the need for a concerted research effort in this direction.

In summary, we have isolated what we believe to be an important aspect of tropical-cyclone dynamics and have provided a physically plausible interpretation of the results. This interpretation should not be construed as a complete theory. Even though the enthalpy exchange coefficients are held constant in this study, an increase in the surface wind speed brought about by a change in the value of the drag coefficient results in a change in the enthalpy fluxes. To account for the changes in the aggregate forcing of the overturning circulation due to these flux changes would require a theory incorporating the coupling of the (unbalanced) boundary layer with the interior flow. As far as we are aware, no such theory exists at the present time.

7. Acknowledgements

We thank Sarah Jones, Jeff Kepert and an anonymous reviewer for their constructive comments on the original version of this manuscript. RKS and GT acknowledge financial support for hurricane research from the German Research Council (Deutsche Forschungsgemeinschaft). [10:27:25 AM] Michael T. Montgomery: MTM acknowledges the support of Grant No. N0001411Wx20095 from the U.S. Office of Naval Research and NSF AGS-0733380 and NSF AGS-0851077, NOAAs Hurricane Research Division and NASA grants NNH09AK561 and NNG09HG031.

References

Bister M and Emanuel KA. 1998 Dissipative heating and hurricane intensity. *Meteor. Atmos. Phys.*, **65**, 233-240.

Black PG D'Asoro EA Drennan WM French JR Niller PP Sanford TB Terril EJ Walsh EJ Zhang JA 2007 Air-sea exchange in hurricanes. Synthesis of observations from the coupled boundary layer air-sea transfer experiment. *Bull. Amer. Meteorol. Soc.*, **88,** 357-374.

Blackadar AK. 1976 Modelling the nocturnal boundary layer. Third Symp. on Atmospheric Turbulence,

Diffusion and Air Quality. Raleigh NC, *Amer. Meteor. Soc.* 46-49.

Braun, SA Tao W-K. 2000 Sensitivity of high-resolution simulations of Hurricane Bob (1991) to planetary boundary layer parameterizations. *Mon. Wea. Rev.*, **128**, 3941-3961.

Bryan GH Rotunno R. 2009a The maximum intensity of tropical cyclones in axisymmetric numerical model simulations. *Mon. Wea. Rev.*, **137,** 1170-1789.

Bryan GH Rotunno R. 2009b Evaluation of an analytical model for the maximum intensity of tropical cyclones. *J. Atmos. Sci.*, **66**, 3042-3060.

Bui HB Smith RK Montgomery MT Peng J. (M4) 2009 Balanced and unbalanced aspects of tropical-cyclone intensification. *Q. J. R. Meteor. Soc.*, **135**, 1715-1731.

Chen SS Price JF Zhao W, Donelan MA Walsh EJ. 2007 The CBLAST-Hurricane Program and the next-generation fully coupled atmospherewaveocean models for hurricane research and prediction. *Bull. Amer. Meteorol. Soc.*, **88,** 311-317.

Craig GC Gray SL. 1996 CISK or WISHE as a mechanism for tropical cyclone intensification. *J. Atmos. Sci.*, **53**, 3528-3540.

Drennan WM Zhang JA French JR McCormick C Black PB. 2007 Turbulent fluxes in the hurricane boundary layer. Part II: Latent heat fluxes. *J. Atmos. Sci.*, **64**, 1103-1115.

Emanuel KA. 1986 An air-sea interaction theory for tropical cyclones. Part I: Steady state maintenance. *J. Atmos. Sci.*, **43**, 585-604.

Emanuel KA. 1995 Sensitivity of tropical cyclones to surface exchange coefficients and a revised steady-state model incorporating eye dynamics. *J. Atmos. Sci.*, **52**, 3969-3976.

Emanuel KA. 2004 Tropical cyclone energetics and structure. In: Atmospheric Turbulence and Mesoscale Meteorology, E. Fedorovich, R. Rotunno and B. Stevens, Eds. Cambridge University Press, 165 - 191.

French JR Drennan WM Zhang JA Black PB. 2007 Turbulent fluxes in the hurricane boundary layer. Part II: Momentum fluxes. *J. Atmos. Sci.*, **64**, 1089-1102.

Hakim GJ. 2010 The mean state of axisymmetric hurricanes in statistical equilibrium. *J. Atmos. Sci.*, **68**, 1364-1376.

Hill KA Lackmann GL. 2009 Analysis of idealized tropical cyclone simulations using the Weather research and Forecasting model: Sensitivity to turbulence parameterization and grid spacing. *Mon. Wea. Rev.*, **137**, 745-765.

Jordan CL. 1958 Mean soundings for the West Indies area. *J. Meteor.*, **15,** 91-97.

Kepert JD. 2001 The dynamics of boundary layer jets within the tropical cyclone core. Part I: Linear Theory. *J. Atmos. Sci.*, **58,** 2469-2484.

Kleinschmidt E. 1951 Grundlagen einer Theorie der Tropischen Zyklonen. *Arch. Meteorol. Geophys. Bioklimatol.*, **A4**, 5372.

Montgomery MT Smith RK Nguyen SV. 2010 Sensitivity of tropical cyclone models to the surface exchange coefficients. *Q. J. R. Meteor. Soc.*, **136**, 19451953.

Nguyen CM Smith RK Zhu H Ulrich W. 2002 A minimal axisymmetric hurricane model *Q. J. R. Meteor. Soc.*, **128**, 26412661.

Nguyen SV Smith RK Montgomery MT. (M1) 2008 Tropical-cyclone intensification and predictability in three dimensions. *Q. J. R. Meteor. Soc.*, **134**, 563-582.

Persing J Montgomery MT. 2003 Hurricane superintensity. *J. Atmos. Sci.*, **60**, 2349-2371.

Riehl H. 1954 *Tropical Meteorology*. McGraw-Hill, 392pp.

Rotunno R and Emanuel KA. 1987 An air-sea interaction theory for tropical cyclones. Part II: Evolutionary study using a nonhydrostatic axisymmetric numerical model. *J. Atmos. Sci.*, **44**, 542-561.

Shapiro LJ Willoughby H. 1982 The response of balanced hurricanes to local sources of heat and momentum. *J. Atmos. Sci.*, **39**, 378-394.

Shapiro LJ Montgomery MT. 1993 A three-dimensional balance theory for rapidly-rotating vortices. *J. Atmos. Sci.*, **50**, 3322-3335.

Smith RK. 2006 Accurate determination of a balanced axisymmetric vortex. *Tellus*, **58A**, 98-103.

Smith RK Vogl S. 2008 A simple model of the hurricane boundary layer revisited. *Q. J. R. Meteor. Soc.*, **134**, 337-351.

Smith RK Montgomery MT. 2010 Hurricane boundary layer theory. *Q. J. R. Meteor. Soc.*, ,**136**, 16651670

Smith RK Thomsen GL. 2010 Dependence of tropical-cyclone intensification on the boundary layer representation in a numerical model. *Q. J. R. Meteor. Soc.*, **136**, 1671-1685.

Smith RK Montgomery MT and Vogl S. 2008 A critique of Emanuel's hurricane model and potential intensity theory. *Q. J. R. Meteor. Soc.*, **134**, 551-561.

Smith RK Montgomery MT Nguyen SV. 2009 Tropical cyclone spin up revisited. *Q. J. R. Meteor. Soc.*, **135,** 1321-1335.

Thomsen GL Smith RK. 2008 The importance of the boundary layer parameterization in the prediction of low-level convergence lines. *Mon. Wea. Rev.*, **136**, 2173-2185.

Vigh JL Schubert W. 2009 Rapid development of the tropical cyclone warm core. *J. Atmos. Sci.*, **66**, 3335-3350.

Vogl S Smith RK. 2009 A simple model of the hurricane boundary layer revisited. *Q. J. R. Meteor. Soc.*, **135,** 337-351.

Willoughby HE. 1979 Forced secondary circulations in hurricanes. *J. Geophys. Res.*, **84**, 3173-3183.

Zhang JA Black PB French JR Drennan WM. 2008 First direct measurements of enthalpy fluxes in the hurricane boundary layer: The CBLAST result. *Geophys. Res. Lett.*, **35**, L14813, doi:10.1029/2008GL034374.

Zhang JA Marks FD Montgomery MT Lorsolo S. 2010 Estimation of turbulence characteristics of eyewall boundary layer of Hurricane Hugo (1989) *Mon. Wea. Rev.*, in press.

Zhang D-L Liu Y Yau MK. 2001 A multi-scale numerical study of Hurricane Andrew (1992). Part IV: Unbalanced flows. *Mon. Wea. Rev.*, **129**, 92-107.